STEM CELLS TRANSLATIONAL MEDICINE®

TISSUE ENGINEERING AND REGENERATIVE MEDICINE

Translating Periosteum's Regenerative Power: Insights From Quantitative Analysis of Tissue Genesis With a Periosteum Substitute Implant

SHANNON R. MOORE,[a] CÉLINE HEU,[b,c] NICOLE Y.C. YU,[b] RENEE M. WHAN,[c] ULF R. KNOTHE,[d] STEFAN MILZ,[e] MELISSA L. KNOTHE TATE[b]

Key Words. Periosteum • Mesenchymal stem cell • Tissue genesis • Regenerative medicine • Tissue engineering

[a]Department of Biomedical Engineering, Case Western Reserve University, Cleveland, Ohio, USA; [b]Graduate School of Biomedical Engineering and [c]Biomedical Imaging Facility, Mark Wainwright Analytical Centre, University of New South Wales, Sydney, New South Wales, Australia; [d]Department of Orthopaedic Surgery, Cleveland Clinic, Cleveland, Ohio, USA; [e]Anatomische Anstalt, Ludwig Maximilians University of Munich, Munich, Germany

Correspondence: Melissa L. Knothe Tate, Ph.D., Professor and Paul Trainor Chair of Biomedical Engineering, Graduate School of Biomedical Engineering, University of New South Wales, Samuels 509, UNSW Sydney 2052, New South Wales, Australia. E-Mail: m.knothetate@unsw.edu.au

Received January 7, 2016; accepted for publication May 13, 2016; published Online First on July 27, 2016.

1066-5099/2016/$20.00/0

http://dx.doi.org/10.5966/sctm.2016-0004

ABSTRACT

An abundance of surgical studies during the past 2 centuries provide empirical evidence of periosteum's regenerative power for reconstructing tissues as diverse as trachea and bone. This study aimed to develop quantitative, efficacy-based measures, thereby providing translational guidelines for the use of periosteum to harness the body's own healing potential and generate target tissues. The current study quantitatively and qualitatively demonstrated tissue generation modulated by a periosteum substitute membrane that replicates the structural constituents of native periosteum (elastin, collagen, progenitor cells) and its barrier, extracellular, and cellular properties. It shows the potentiation of the periosteum's regenerative capacity through the progenitor cells that inhabit the tissue, biological factors intrinsic to the extracellular matrix of periosteum, and mechanobiological factors related to implant design and implementation. In contrast to the direct intramembranous bone generated in defects surrounded by patent periosteum in situ, tissue generation in bone defects bounded by the periosteum substitute implant occurred primarily via endochondral mechanisms whereby cartilage was first generated and then converted to bone. In addition, in defects treated with the periosteum substitute, tissue generation was highest along the major centroidal axis, which is most resistant to prevailing bending loads. Taken together, these data indicate the possibility of designing modular periosteum substitute implants that can be tuned for vectorial and spatiotemporal delivery of biological agents and facilitation of target tissue genesis for diverse surgical scenarios and regenerative medicine approaches. It also underscores the potential to develop physical therapy protocols to maximize tissue genesis via the implant's mechanoactive properties. STEM CELLS TRANSLATIONAL MEDICINE *2016;5:1739–1749*

SIGNIFICANCE

In the past 2 centuries, the periosteum, a niche for stem cells and super-smart biological material, has been used empirically in surgery to repair tissues as diverse as trachea and bone. In the past 25 years, the number of articles indexed in PubMed for the keywords "periosteum and tissue engineering" and "periosteum and regenerative medicine" has burgeoned. Yet the biggest limitation to the prescriptive use of periosteum is lack of easy access, giving impetus to the development of periosteum substitutes. Recent studies have opened up the possibility to bank periosteal tissues (e.g., from the femoral neck during routine resection for implantation of hip replacements). This study used an interdisciplinary, quantitative approach to assess tissue genesis in modular periosteum substitute implants, with the aim to provide translational strategies for regenerative medicine and tissue engineering.

INTRODUCTION

For well over 2 centuries [1–4], surgeons have used the periosteum, a hyperelastic soft tissue sheath that covers all nonarticular bone surfaces, to repair and regenerate tissue. Surgical applications of periosteum include treatment of retinal detachment with scleral buckle [5]; treatment of cleft lip and palate [6–12]; dental [13–15] and muscle hernia [16] repair; treatment of defects in cartilage [17–24], laryngeal and tracheal walls [25, 26], and bone [27–29]; and treatment of fractures in children [30, 31]. Interest in translating the regenerative capacity of the periosteum has burgeoned in recent years (Fig. 1), from early and growing interest in uses of periosteum in tissue engineering during the past two decades to increasing interest in its application to regenerative medicine. Although the use of native periosteum in vivo offers a powerful biological tool for surgical treatment, the amount of available healthy periosteum is a limiting factor in its use. This has provided the impetus for the development of periosteum

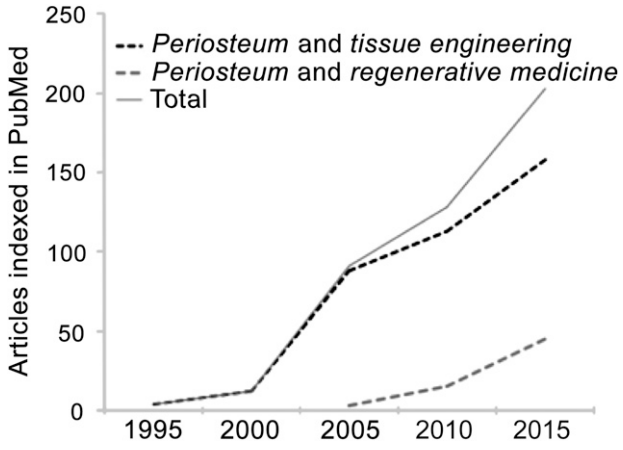

Figure 1. A PubMed search for the keywords "periosteum and regenerative medicine" or "periosteum and tissue engineering" yielded more than 215 articles published in the past 5 years (2010–2015), compared with 109, or roughly half that number, in the 5 years before (2005–2010) and 70 in the 5 years before that (2000–2005).

substitutes. Despite recent progress in the field, there is an acute need for quantitative measures to develop efficacy-based translational strategies for native periosteum as well to have a baseline for comparison of periosteum substitutes.

Periosteal tissue exhibits remarkable smart properties, including direction- and flow rate-dependent permeability [32–34] and increased failure strength and energy absorption to failure at increased rates of loading [34, 35]. These respective properties control molecular traffic between muscle and bone [33, 36] and imbue bone with paradoxically higher failure strength compared with bone denuded of periosteum [35]. In addition to its smart material properties, periosteum serves as a niche for mesenchymal stem cells throughout life [37–39]. Recent studies have opened the possibility to banking of periosteal tissues (e.g., from the femoral neck during its routine resection for implantation of hip replacements [39]). Yet few quantitative studies have been carried out to determine how best to use this banked tissue for regenerative medicine purposes at a later time in the patient's life.

Attached like Velcro to bone surfaces via collagenous Sharpey's fibers, periosteum is prestressed in situ [33, 34]. Separation of the Sharpey's fibers changes the stress state of periosteum [40]. Such changes in periosteum's intrinsic stress change the conformation of collagen fibrils within the tissue concomitant with changes in the shape of periosteal cell nuclei; these changes are hypothesized to regulate quiescence of the progenitor cells inhabiting periosteal tissue, also called periosteum-derived cells (PDCs) [41]. PDCs isolated from humans express mesenchymal stem cell (MSC) surface markers, including CD73, CD90, and CD105, more consistently and at significantly higher levels than seen with bone marrow stromal cells (BMSCs), which are MSCs from the bone marrow niche. In such analyses, human PDCs lend themselves to flow cytometry analysis because of the absence of surface-marker expression in nonhuman large vertebrates such as sheep [38]. Yet ovine studies are particularly helpful for assessing efficacy of tissue genesis and healing in models of critical-sized defects. In a series of ovine studies that implemented periosteum in the presence or absence of bone graft, factors intrinsic to periosteum alone were not only sufficient but also more efficient in generating tissue than when used in combination with bone graft, the current standard of care (Fig. 2A–2C) [42–46].

To replicate these intrinsic properties of native periosteum, we developed a modular periosteum substitute membrane designed to mimic cellular, biochemical, and barrier properties of periosteum [44, 47, 48]. The current study aimed to quantify tissue genesis in these periosteum substitute membranes and, ultimately, to provide translational strategies for regenerative medicine and tissue engineering. The replacement periosteum was designed to provide directional (outside→in) and spatiotemporal delivery of biological factors, as well as barrier functions to guide delivery to the center of the defect. Composed of U.S. Food and Drug Administration (FDA)-approved silicone sheeting, the membrane is highly elastic. Inclusion of collagen, the primary structural protein found in the periosteum [49], mimics the membrane's extracellular matrix (ECM) and native cellular environment. Additionally, autologous periosteal osteoprogenitor cells and periosteum strips were included in the implant. The current study was designed to quantify the relative effects of collagen membranes, periosteal cells seeded on collagen membranes, and periosteal strips on defect infilling in an ovine model. An isotropic control membrane served as a control. Four unique groups, including the control group (group 1) were tested, with five animals per groups (Fig. 2D–2I; Table 1).

Materials and Methods

We qualitatively and quantitatively assessed tissue regeneration outcomes after a 16-week experimental treatment with each of the implant combinations. High-resolution imaging and histomorphometry were used to determine the quantity and distribution of regenerated tissue, distinguished as cartilage or mineralized tissue, within the defect zone and in relation to the periosteum substitute membrane. Ultimately, we aimed to assess these data with the goals of replacing periosteal function and translating substitute periosteum implants in the context of regenerative medicine.

Membrane Manufacture

Techniques used to produce and implant the periosteal replacement are outlined briefly in the following section and were described in more detail in a previous publication on development and testing of the implant cum delivery device [44, 48]. The general concept was to create a modular membrane implant with pockets, into which biological factors (isolated autologous periosteum-derived progenitor cells and periosteal strips) are tucked. The implant comprises FDA-approved silicone elastomer sheeting with outer and inner layers. The inner layer is perforated to create a gradient of holes, with the highest concentration near the center of the defect region. An outer unperforated layer is then sewn, using suture as thread, to the perforated layer to create a long sleeve (3.5 cm $\times$ 10 cm) with four 2-cm-wide pockets (Fig. 2D–2I). In this way, the periosteum substitute implant exhibits a modular design for inclusion of periosteal, biological, or other factors into the pockets of the sleeve, which are arranged for factor delivery with spatial and vectorial (controlling magnitude and direction) control.

Preparation for Implantation

In the current study, just before surgical implantation, small sheets comprising combinations of collagen and periosteal

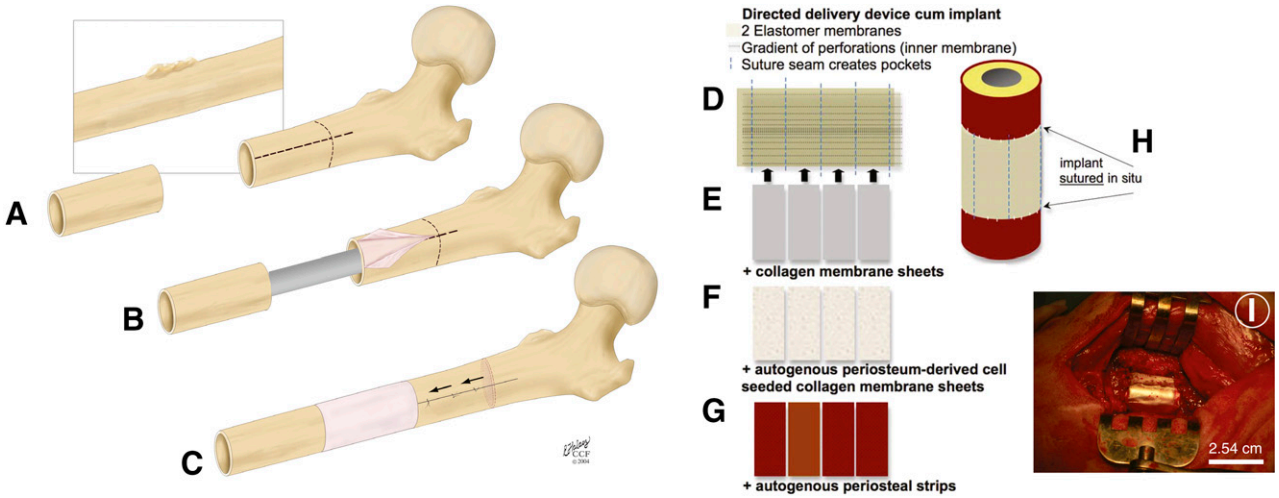

Figure 2. Harnessing the regenerative power of periosteum using native periosteum tissue in situ and/or periosteum substitute membranes. **(A–C):** The one-stage bone-transport procedure for treatment of bone defects, such as those occurring after tumor resection. **(A, B):** The periosteum is elevated off healthy cortical bone (light pink), which is then osteotomized and transported distally over an intramedullary nail **(C)**. The periosteum remains attached proximally and is sutured around created defect. Adapted from [42]. **(D–I):** Delivery device for periosteal factors. **(D):** The periosteum substitute implant comprises two layers of silicone elastomer that are sutured together to create pockets and are sandwiched around collagen membrane sheets **(E)**, collagen sheets seeded with periosteal cells **(F)**, or autologous periosteal strips **(G)**. **(H, I):** The complete implant is sutured in situ to itself and to neighboring periosteum. Adapted from [44].

Table 1. Summary of experimental groups in ovine model (n = 5 per group)

Group	Surgical membrane	Collagen	Periosteal factor
1	–	–	–
2	+	+	–
3	+	+	+ cells
4	+	–	+ periosteal strips

+, presence of specific factors, including the surgical membrane collagen and factors intrinsic to periosteum (cells alone and periosteal strips); –, absence of specific factors, including the surgical membrane collagen and factors intrinsic to periosteum (cells alone and periosteal strips).

factors were inserted into the pockets of the periosteum substitute membrane sleeve. Group 2 included the periosteum substitute membrane with collagen sheets tucked into the pockets (Fig. 2E). Group 3 included collagen sheets seeded with autologous PDCs tucked into the pockets; for this purpose, periosteum from the femoral mid-diaphysis block, removed to create the defect, was resected and incubated in collagenase per protocols implemented previously to isolate PDCs from ovine and human periosteum [38, 44, 50]. After filtering to remove fibrous tissue, PDCs were seeded onto the precut collagen sheets and cultured overnight. The collagen sheets seeded with PDCs were then tucked into the periosteum substitute membrane's pockets (Fig. 2F). Finally, group 4 included autologous periosteal strips harvested from the bone removed to create the critical-sized defect, trimmed, and tucked into the periosteum substitute membrane's pockets (Fig. 2G).

Experimental Surgery and Study Design

Surgical protocol followed that of the one-stage bone-transport procedure (Fig. 2A–2C) [27, 42]. All animal experimentation procedures were carried out in accordance with the Institutional Animal Care and Use Committee of the Canton of Grisons, Switzerland. Sheep from a matched cohort of similar age were anesthetized, the intramedullary (IM) canal was reamed, a 2.54-cm defect was created at the mid-diaphysis, and a stainless steel IM nail was inserted and locked. The periosteum replacement device was wrapped around the created defect site and sutured at the lateral aspect as well as to healthy periosteum proximal and distal to the defect (Fig. 2H, 2I). During the 16-week experimental duration, sheep were allowed to bear load on the operated side (while supported by a sling during the first 2 weeks after surgery) and to graze normally. Intravital fluorochromes were administrated at specific time points after surgery, including calcein green (1 and 2 weeks after surgery), xylenol orange (3 and 4 weeks after surgery), Terramycin (yellow; Pfizer, New York, NY, http://www.pfizer.com) (8 and 12 weeks after surgery), and Procion Red (Sigma-Aldrich, St. Louis, MO, http://www.sigmaaldrich.com) (immediately before euthanasia) as per previous protocol [42].

Histological Preparation and Sectioning

After euthanasia, the experimental bone was resected and imaged by using micro computed tomography (μCT) imaging. The femur and surrounding soft tissue were fixed and embedded in poly(methyl methacrylate) (PMMA) for undecalcified histology, for optimal preservation of hard and soft tissue geometry. For each femur, three serial cross-sectional samples were taken by using a diamond wire saw (Well Precision Diamond Wire Saw 6234, Well Precision Diamond Wire Saws Inc., Norcross, GA, http://www.welldiamondwiresaws.com/) because the IM nail was left in situ to preserve regenerated tissue. These cross-sectional samples, of approximately 6.5-mm thickness, were cut sequentially to span the entirety of the defect site. Both proximal and distal sides of each sample were polished by using sandpaper of increasing grit on a rotating polisher with a constant stream of deionized water (EcoMet 4000, Buehler,

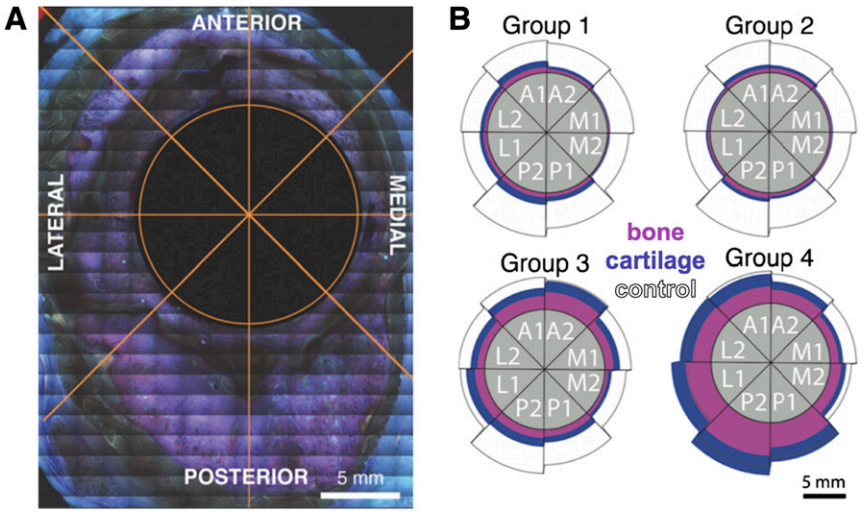

Figure 3. Spatial distribution of tissue genesis. **(A):** For digital processing and analysis of high-resolution image collages, an octant was overlaid over the entire cross-section, centered on the intramedullary nail cross-section. **(B):** Total tissue genesis as well as the relative amounts of mineralized (pink) and cartilage tissue (blue) were measured in each sector, including lateral (L1, L2), anterior (A1, A2), medial (M1, M2), and posterior (P1, P2) aspects. The gray circle represents the intramedullary nail (1.5 cm diameter), and the black-outlined white areas show the comparative control area to demonstrate normal tissue distribution. Group 4 showed a greater area of regenerated tissue in the lateral and posterior quadrants than that observed in a normal femur.

Lake Bluff, IL, http://www.buehler.com/). Anatomical orientation (lateral, medial, proximal, distal) was carefully tracked throughout preparation, as determined by aligning PMMA-embedded tissue blocks with high-resolution radiographic images (Faxitron, Tucson, AZ, http://www.faxitron.com).

To distinguish collagen, cell nuclei, and mineralized tissue, a subset of thick sections were stained with Giemsa and eosin. This stain dyes cell nuclei and connective tissue dark blue and mineralized tissue (bone) pink. After etching with 1% formic acid, the sections were submerged in a 15% Giemsa solution for 30 minutes at 55°C, and rinsed liberally with deionized water, followed by 1 minute in a 1% eosin solution at room temperature. The sections were then dehydrated with ethanol washes of 70%, 96%, and 100%. Finally, additional, approximately 100-μm-thick, sections were prepared (unstained) for reflective and confocal imaging of the entire cross-section at high resolution.

Optical Imaging and Analysis

High-resolution collages of Giemsa- and eosin-stained sections were obtained by using an epifluorescent microscope with an automated, computerized stage (Leica DMIRE2, Leica Microsystems, Wetzlar, Germany, http://www.leica-microsystems.com). Both sides of the thick samples were imaged in reflectance with broad-spectrum ultraviolet excitation at $\times$5 magnification. A custom control algorithm allowed for images to be taken in a precise sequence to allow for direct collaging, wherein each cross-section collage comprised approximately 300 captured views. Collaging allowed for high-resolution visualization of tissue regeneration on multiple length scales.

Collages were imported into image processing software (Adobe Photoshop CS5, Adobe Systems Inc., San Jose, CA, http://www.adobe.com), wherein regenerated tissue between the membrane and nail were manually isolated from surrounding soft tissue and membrane material. The single observer was blinded to group number, and samples were randomized to prevent bias. Ectopic bone, although not observed in all samples or groups, was excluded from newly regenerated tissue measures. Each cross-sectional collage was divided virtually into eight 45° sectors, oriented along the lateral-medial line (Fig. 3A). The pink-stained mineralized tissue was thresholded from blue-stained cartilage tissue templates, and each was saved as a separate binarized image. Black and white images were imported to ImageJ software, version 10.2 (National Institutes of Health, Bethesda, MD, https://imagej.nih.gov/ij/), where pixel calibrations were used to compute area measures of total tissue callus, mineralized tissue, and cartilage as a function of radial section (octant location) and serial location (proximodistal).

Cross-sections revealing native bone at the distal and proximal edges of the defect (i.e., bone that had not been regenerated during the experiment), visible as densely organized cancellous bone exhibiting bright pink stain, were excluded from quantitative analysis. The described preparations resulted in greater than 27 surfaces for all four groups. Because of the anticipated high variability of outcome measures intrinsic to in vivo experiments, an Anderson-Darling test (MiniTab 16, MiniTab, State College, PA, https://www.minitab.com) was carried out and revealed significant deviations from normal distribution. Nonparametric Kruskal-Wallis, Mann-Whitney, and Spearman correlation tests were therefore used to perform analyses, for which p values less than 0.05 were defined as indicating a statistically significant difference.

Reflective and Fluorochrome Imaging Analysis

Images of unstained, 100-μm-thick sections were acquired in high resolution by using a Nikon A1 laser confocal microscope (Nikon, Tokyo, Japan, http://www.nikon.com/) with motorized stage that enabled automated tiling of image sets from multipoint positions for large specimen coverage. IM nails were imaged in reflection mode, and fluorochromes were imaged by tuning for the specific excitation and emission characteristics of the fluorochromes administered during the study. Images were stitched together

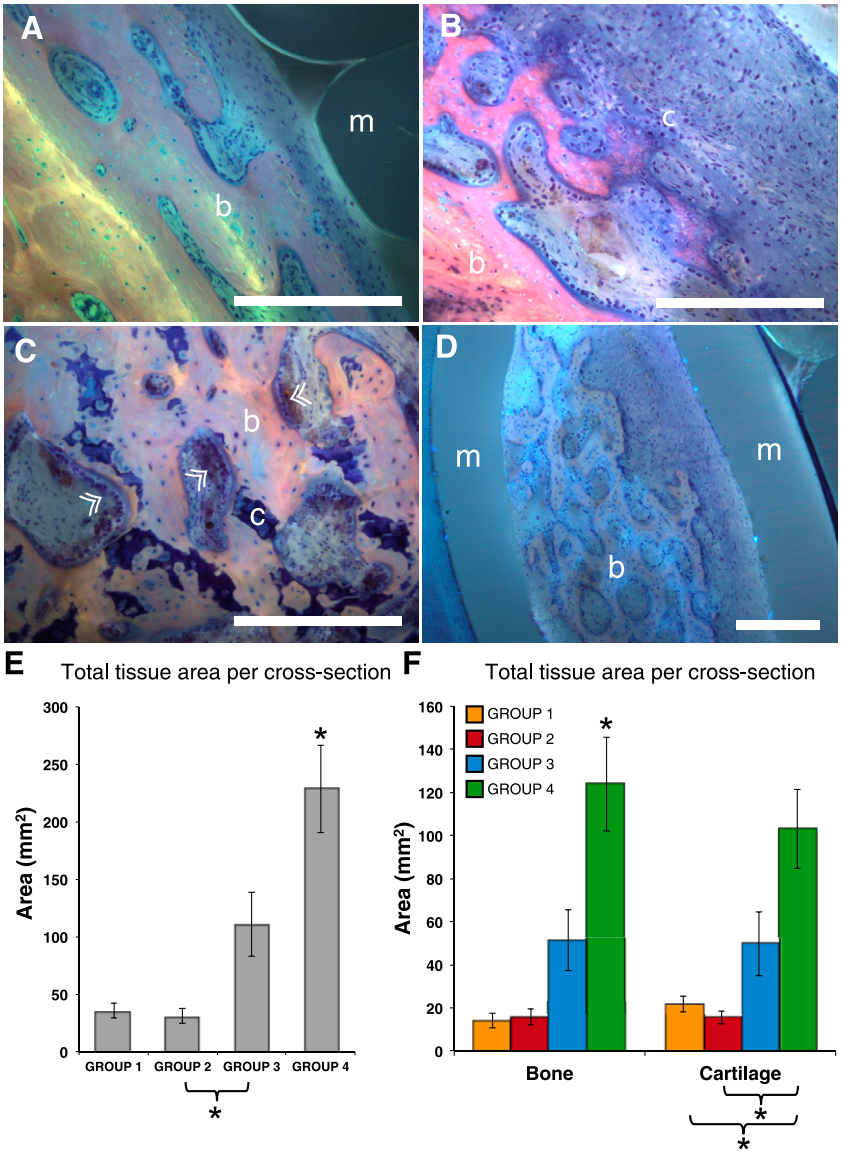

Figure 4. Tissue genesis within the defect occurs primarily via an endochondral ossification mechanism. **(A):** Mineralized bone (pink-staining) was not observed to interdigitate with the membrane (gray-blue) but typically interfaced via a layer of cellular fibrous tissue. The fibrous tissue was not observed to infill small-radius concavities, likely because of the hydrophobic properties of silicone. **(B):** Indirect, endochondral bone formation via mineralization of a cartilaginous template. **(C):** Cartilaginous remnants are apparent in remodeling bone tissue, where osteoblastic bone apposition is noted in several areas (arrowheads). **(D):** Islands of bone were occasionally observed within folds of the membrane. Scale bar for **A–D** = 100 μm. **(E):** Total tissue (mineralized and cartilage) generated reveals a significantly greater area of regenerated tissue in group 4 (periosteal strips). **(F):** Summary of mineralized bone and cartilage tissue per cross-section shows relative distribution of bone and cartilage tissue for each group. Inclusion of periosteum strips (group 4) resulted in significantly greater bone formation than all other groups and significantly greater cartilage formation than all groups except cell-seeded collagen strips (group 3). Error bars represent SEM. $*$, significant at $p < .05$. Abbreviations: b, bone; c, cartilage; m, elastomeric membrane.

across the entire cross-section of the middiaphyseal defect, enabling visualization of characteristic regions comprising stainless steel and periosteum substitute implants, bone tissue with time-indicative fluorochromes, and autofluorescent fibrous tissue at some bone-implant interfaces.

Results

Quantitative measurements as well as qualitative observations of μCT images indicated significantly greater bone regeneration at 16 weeks after surgery with inclusion of autologous periosteal strips tucked into the periosteum substitute (group 4). Seeding of periosteal cells on collagen sheets that were tucked into the periosteum substitute (group 3) resulted in significantly greater total tissue area compared with treatment with simple collagen sheets tucked into the periosteum substitute (group 2). Inclusion of collagen sheets in the implant's pockets did not result in increased bone formation compared with the isotropic control membrane, indicating that periosteal cells plus factors intrinsic to the periosteum are crucial for bone regeneration processes. Ectopic bone formation was visibly greater in groups treated with the periosteum

substitute membrane that incorporated collagen sheets alone; in addition to ectopic bone within the muscle, bone regeneration in this group was often observed outside of the defect zone and the periosteum substitute implant.

Qualitative Histology and μCT

On the basis of observation of collages from cross-sections representing all groups (Fig. 4), ossification occurred predominantly via an endochondral mechanism, where a cartilaginous template subsequently mineralizes into loosely organized bone. Bone formation appeared similar across all treatment groups. Most bone formation occurred between the inner membrane layer and the intramedullary nail, with few sites of bone formation between the periosteum substitute membrane layers or external to the membrane (between the outer membrane layer and surrounding soft tissue) (Fig. 4A–4D).

Although quantitative analysis of μCT data was not possible because of beam-hardening artifacts created by the in situ intramedullary nail, regenerated tissue volumes could be measured and compared quantitatively. Tissue genesis in groups 1 and 2 appeared dependent on proximity to native bone both proximal and distal to defect (supplemental online Fig. 1). More robust tissue regeneration volumes were observed in groups 3 and 4 and appeared evenly distributed throughout the defect space, independent of proximity to native bone at the distal and proximal edges of the defect.

Quantitative Measures of Histology

The Kruskal-Wallis test provides a one-way comparison of both mineralized and cartilage tissue areas by group, showing significant differences ($p < .0003$ and $p = .0039$, respectively) indicate a real effect of membrane design on respective mineralized and cartilaginous tissue generation. Total regenerated tissue (cartilage + mineralized) area was compared for each group by using a two-sample nonparametric Mann-Whitney test (Fig. 4E), revealing significantly greater regenerated tissue area in group 4 (periosteal strips) compared with all other groups. Additionally, group 3 (collagen + periosteal cells) showed significantly greater regenerated tissue area than group 2 (collagen only), but not group 1 (isotropic membrane). Assessing tissue types, animals in group 4 produced significantly more mineralized tissue than other groups. The area of cartilage in group 4 is significantly greater than that resulting from groups 1 and 2, which do not include a cellular periosteal component, although not significantly greater than group 3 (Fig. 4F).

Large interindividual differences were observed in measurements of mineralized and cartilage tissue, both within and between groups (Fig. 5). As comparison, the approximate normal cross-sectional area of bone at the mid-diaphysis in ovine femur is 220 mm^2, measured from sections through native bone proximal and distal to the defect site. One sheep from group 3 and two sheep from group 4 showed a total area of mineralized tissue greater than the cross-sectional area of normal bone.

Sector analysis data revealed both mineralized bone and cartilage formation oriented mainly along the anterior-posterior axis (Fig. 3B). The Spearman correlation indicated a significant correlation with anatomical octant for both mineralized ($p < .001$) and cartilage tissue ($p = .014$) for group 4, although no other groups displayed significant correlations.

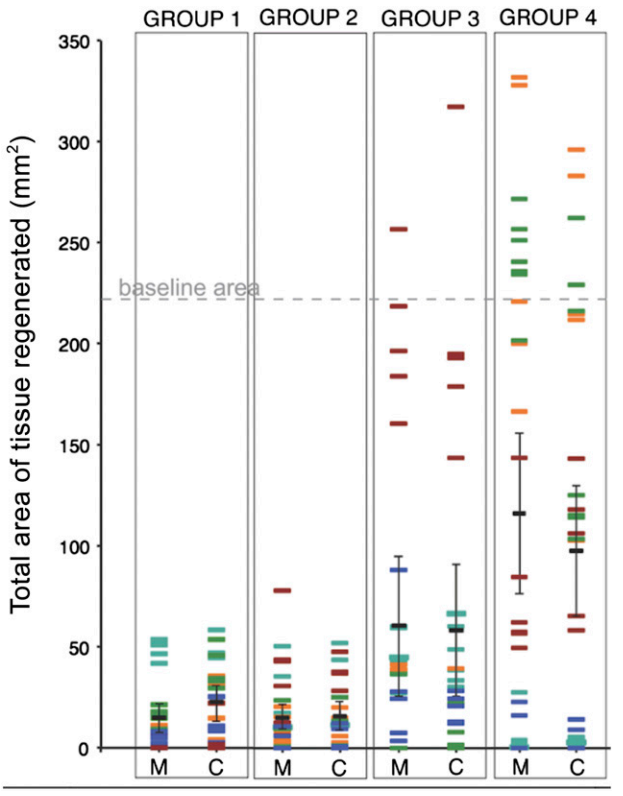

Figure 5. Individual regenerated area per cross-section by group. Separate colors within a group represent individual sheep, with 5 sheep per group (total, 20). Black bars show mean of all cross-sections from group. Dotted line indicates bone area of baseline control bone cross-section, removed to create the defect. Error bars represent 95% confidence interval of mean. Abbreviations: C, cartilage tissue; M, mineralized.

Fluorochrome Assessment of Cortical Collages

The dynamics and emergent architecture of tissue genesis by stem cells was highly dependent on the local environment defined by the stiff, inner (stainless steel IM nail surface) and flexible, outer (exterior surface of silicone implant) boundaries as well as the presence of trophic factors intrinsic to experimental groups. Interestingly, the stress state of the silicon implant appeared to affect the resistance properties of the inner and outer envelopes for tissue genesis, where taut boundaries (Fig. 6) showed smaller volume of proliferative tissue genesis than slack elastomer regions with ample folds (Fig. 6). Greater bone mineralization was shown in groups 3 and 4, which supported μCT observations. Interestingly, ectopic bone formation was observed in group 2 (implant + collagen), with bone formation external to the implant boundary and within muscle.

Discussion

An abundance of clinical studies provide empirical evidence for periosteum's regenerative power when applied in diverse surgical procedures. The current study quantitatively and qualitatively demonstrates the potentiation of the periosteum's regenerative capacity through the progenitor cells that inhabit the tissue, biological factors intrinsic to the ECM of periosteum, and mechanobiological factors related to implant design and implementation. The novel periosteum substitute membrane was tested to

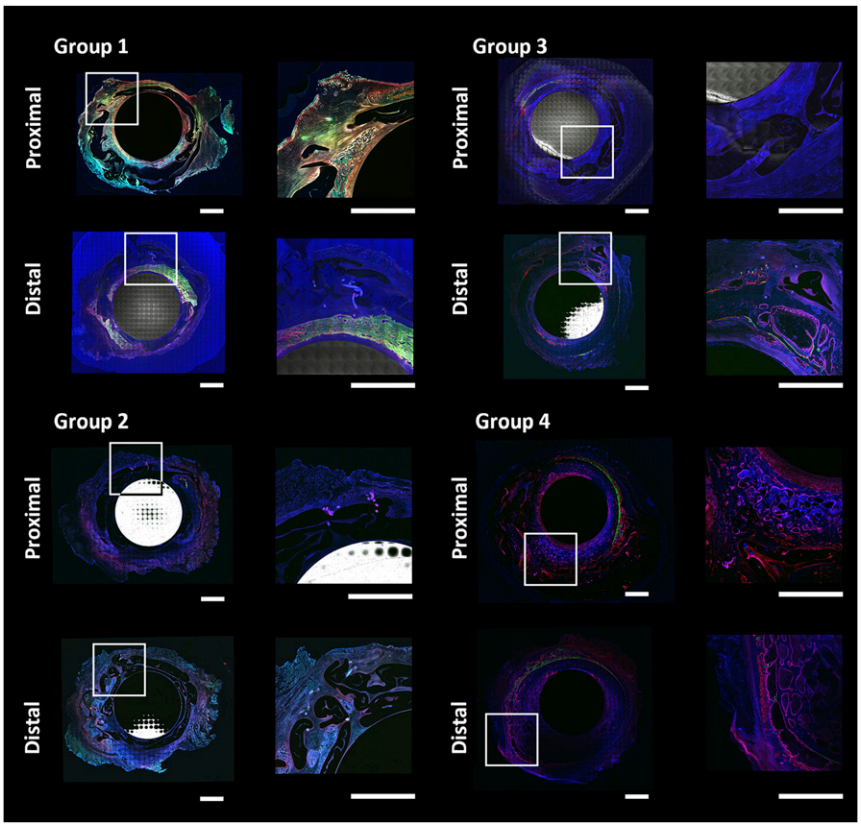

Figure 6. Representative cross-section (collage of high-resolution laser scanning fluorescence images) from each group, showing relationship between tissue genesis and bounding surfaces. Shown is the stainless steel intramedullary nail in the center and silicone elastomer membrane bounding the defect, with tissue genesis within and outside membrane surfaces but not between folds. Fluorescence shows tissue genesis over time, with green indicating tissue generated between 1 and 2 weeks after surgery; orange, 3 and 4 weeks; yellow, 8 and 12 weeks; and red, perfusion (immediately before euthanasia). Elastomer membrane is visible in gray and sutures as discrete blue circles (orthogonal to plane of image) and lines (in plane) in zoomed-in insets. Scale bar = 0.5 cm.

replicate the barrier, extracellular, and cellular properties of native periosteum. In contrast to the direct intramembranous bone generated in defects surrounded by patent periosteum in situ, tissue generation in bone defects bounded by the periosteum substitute implant occurred primarily via endochondral mechanisms where cartilage was first generated and then converted to bone. In addition, in defects treated with the periosteum substitute, tissue generation was highest along the anteroposterior axis of the defect cross-section, corresponding to the major centroidal axis, which is most resistant to prevailing bending loads. Finally, most mineralized tissue persisting 16 weeks after surgery was located within the defect, between the inner surface of the periosteum substitute and the outer surface of the IM nail, which filled the medullary cavity. Taken together, these data indicate the possibility of designing modular periosteum substitute implants that can be used for diverse surgical scenarios targeting different tissue types and regenerative medicine approaches.

Incorporation of periosteal cells and periosteal strips in conjunction with a novel periosteal replacement membrane designed to replicate the barrier, extracellular, and cellular properties of native periosteum improved tissue generation in the ovine critical-sized defect model. Specifically, the inclusion of periosteal strips harvested from the denuded bone segment resulted in maximal bony bridging compared with membranes incorporating periosteal cells seeded on collagen, collagen alone, and an isotropic control membrane. Measured in cross-section, treatment with membrane incorporating periosteal strips resulted, on average, in approximately 125 mm^2 of mineralized bone regenerated area compared with a mean mineralized area of 220 mm^2 in normal ovine femur cross-sections. These data indicate the beneficial role of replacing cellular and extracellular functions of periosteal tissue at the defect site. Given unlimited resources, additional groups, including a collagen membrane group with periosteal strips (as well as a periosteal strip group with PDCs seeded on the inner surfaces), would have fully addressed all permutations of the variables studied. The results of the current study point toward a perhaps underappreciated role of ECM intrinsic factors in the regenerative capacity of the periosteum and have provided inspiration for current and follow-on studies.

Compared with previous experiments using the one-stage bone transport procedure, in which all treated defects (n = 7 per group) were bridged, the use of excised periosteal strips resulted in an overall less robust healing outcome, with 3 of 5 treated defects demonstrating marked healing [42]. The full excision necessary to remove periosteum for transplant severs the nervous, vascular, and lymphatic connections. Although periosteum does grow back in denuded areas with time [51], loss of a patent blood supply in excised periosteum may explain its diminished regenerative capacity compared with intact tissue [52, 53]. Inclusion of

periosteal strips in the modular implant resulted in significantly better outcomes than did inclusion of collagen membranes seeded with progenitor cells; factors intrinsic to the periosteum may account for the significantly improved regenerative capacity of periosteal transplants over progenitor cells seeded on collagen.

Qualitative histology indicates that bone and cartilage forms in the space between the membrane and stabilizing intramedullary nail via a predominant endochondral mechanism, which is typical for periosteally mediated bone regeneration reported in the literature [54–56], but this finding contrasts with previous observations of intramembranous bone formation in defects bounded by patent periosteum [42]. In the absence of the endosteum and medullary vascular supply, which is filled by the IM nail in the currently used critical-sized defect model, the periosteum substitute implant delivered the periosteal cells and biological factors intrinsic to the periosteal strips, effectively delivering factors with regenerative capacity in a vectorial manner (i.e., controlling the direction and magnitude of delivery).

Seeding of periosteally isolated cells on collagen sheets resulted in an increased total tissue regenerated volume over the control group, with a robust healing outcome in one defect. Comparison of mean mineralized and cartilage tissue areas revealed no significant differences between groups seeded collagen membranes and collagen membranes alone. In the future it would be interesting to study the effect of not only collagen per se but also collagen bioavailability on its osteogenic potential. The collagen membrane used in the current study comprised BioMend adsorbable collagen membranes for guided tissue repair of the dental gingiva, developed from bovine Achilles tendon by Integra LifeSciences Holding Corp. (Plainsboro Township, NJ, http://www.integralife.com/) [57], which serve as occlusive or bounding membranes during reconstructive surgeries. Side-by-side comparison of six such commercially available occlusive membranes (Bio-Gide, Geistlich Biomaterials, Wolhusen, Switzerland, http://www.geistlich-na.com; GORE-TEX, W.L. Gore and Associates, Newark, DE, http://www.gore.com; GENTAFOIL resorb, Advanced Medical Solutions Group, Winsford, UK, http://www.admedsol.com/; RESODONT, Advanced Medical Solutions Group; BioMend, Zimmer Biomet, Warsaw, IN, http://www.zimmerbiomet.com/; and BioMend Extend Membranes, Zimmer Biomet) showed significant differences in attachment, proliferation, and osteogenic differentiation of MSCs on the different membranes; the researchers concluded that Bio-Gide and RESODONT membranes are most conducive to bone regeneration in an in vitro setting [58, 59]. Similarly, a different in vitro study conducting a side-by-side comparison of eight commercially available guided bone generation membranes showed significant differences in migration rates of mouse osteoprogenitor cells depending on i.a. membrane composition, surface topography, and spatial structure (including porosity and fibrillar architecture), as well as wettability [59]. While the authors of this study conjecture that collagen containing membranes may be used clinically to promote "formation of a thin osteoblastic cell layer to eventually enhance bone regeneration," side-by-side comparison of bone regeneration in vivo would be needed to prove this [59]. In addition, recent in vitro studies indicated a positive effect of incorporating collagen type I in hydrogels designed to guide stem cell differentiation toward osteogenesis [60]. Such wide variances in in vitro results using different formulations of collagen of varying bioavailability underscore the need for controlled in vivo comparative models using a common critical-sized bone defect model as well as the side-by-side comparison of periosteum substitutes incorporating endogenous ECM structural proteins.

Although the one successfully bridged defect with isolated cells reveals the potential of cell-based treatments, further development of isolation and seeding methods may be needed. Studies of PDCs isolated from humans using identical protocols have demonstrated their effective equivalence to BMSCs [38]; because of a paucity of cell surface markers for ovine cells, it is not currently possible to validate this finding in the ovine model, which has distinct advantages for study of tissue genesis and healing in critical-sized defects, such as the current study. In addition, isolation and preservation as well as banking protocols will need to be developed and tested for the method to be translated to human patients. For example, enzymatic digestion with collagenase may result in cell loss or damage compared with egression methods of cell isolation [38, 50]; isolation methods themselves may also influence the subpopulation of cells acquired because enzymatically released cells show significant differences in surface markers compared with those egressing from human periosteum [50]. In addition, intersubject variability may affect outcomes because recent studies in humans indicate high interindividual variability in differentiation capacity of periosteum-derived cells from aged, osteoarthritic donors [38]. In addition, follow-on studies will address the role of cell density and specific factors, such as vascular endothelial growth factor and bone morphogenetic protein (BMP) on cell egression, proliferation, and differentiation, as well as extracellular matrix formation.

Across all specimens from groups not delivering periosteal factors (groups 1 and 2), tissue regeneration near the border of the defect site proximally and distally indicates cellular ingression from healthy tissues, consistent with other large animal, critical-sized defect model stabilized with IM nails [61]. In these two groups, it is likely that factors responsible for robust bridging migrate inward from the distal and proximal edges of the defect. However, in groups delivering periosteal factors (groups 3 and 4), tissue also emanates radially from the outside inward, indicating cellular ingression inward from the flow-directing replacement periosteal membrane. Recent experiments with perforated barrier membranes used for guided bone regeneration may offer distinct advantages over total cell-occlusive materials [62], and studies have elucidated the stimuli responsive (so-called smart), directionally dependent inherent permeability of periosteal tissue [32]. Without inclusion of cells or periosteal strips, de novo tissue regeneration is sparse and is characterized by proportions of mineralized tissue and cartilage similar to those observed with delivery of periosteal factors. Taken together, the periosteum substitute membrane demonstrates the capacity to control the magnitude and direction of periosteal factor delivery in a spatiotemporal fashion. Although experimental groups studied in the context of the current study demonstrate the range of outcomes that can be achieved, further tuning of implant parameters will help to determine optimal delivery conditions, including factor type (biochemical or cellular) concentration with respect to density, spatial patterning (guiding gradients), and release kinetics [44, 63]. Furthermore, the intramedullary nail could be coated with factors to achieve concentration gradients (inside → outside) in a direction opposite to that formed by the periosteum substitute (outside → inside) [47, 48].

The lack of increased tissue formation with inclusion of collagen sheets alone in implant pockets presented an unexpected result. We expected collagen membranes alone to promote bone generation within the implant because collagen is the predominant structural protein in the periosteum's extracellular matrix [41, 49, 64] and promotes adhesion of osteoprogenitor cells [65]. Interestingly, ectopic bone formation within the muscle compartment (i.e., external to the outer boundary of the implant) was observed in defects treated with membrane implant and collagen (group 2). Follow-on studies will be necessary to determine whether the collagen membrane per se adsorbs or sequesters factors conducive to ectopic bone formation far from, and external to, the implant (e.g., ectopic bone formation in muscle via BMP-mediated pathways [66] or "muscle-resident mesenchymal progenitor cells, which may be derived from vascular endothelial cells" [67]). MSC homing is highly dependent on local gradients, and creation of targeted tissue genesis compartments through the implant's modular design is an avenue that merits further study.

The current study results using the BioMend absorbable collagen corroborated studies that used similar collagenous membranes for guided bone regeneration, which showed improved osteogenesis over biologically inert polymer membranes [32, 68]. Biomaterials designed for guided bone regeneration aim to promote bone augmentation by a barrier membrane. These materials follow the principle that, under given conditions, cells originating from tissues adjacent to an exclusively provided space can form their parent tissue [68–71].

In addition to biological considerations, the micromechanical environment plays an important role in directing regeneration outcomes [72–76]. The mechanobiological analyses revealed a strong dependence of tissue distribution on major and minor centroidal axes in group 4, with primary sites for healing in anterior and posterior locations, along the axis predominantly exposed to bending. The micromechanical strain environment in the defect site may play a large role in directing the observed cellular response, as observed in the previous study, in which the defect was bounded by patent periosteum in situ and a similar outcome was observed [42]. A recent study correlated net changes in the periosteal strain environment to increased early bone formation within a defect surrounded by periosteum using the one-stage procedure [40]. In addition, the effects of mechanical prestress on periosteum's stem cell niche have recently been characterized quantitatively (specifically, nuclear shape and extracellular matrix architecture). The release of ovine periosteal in situ prestress significantly increased the density of PDCs exhibiting rounded nuclei (within the cambium layer by threefold), and increased degree of collagen crimp (within the fibrous layer by twofold) [41]. Finally, predictive computational models, based on the previous and current study data from the series of ovine studies implementing the one-stage bone transport procedure, probe parametrically which factors exert dominant influence on de novo tissue generation within the defect [63].

The aforementioned approaches aim to elucidate endochondral or intramembranous mechanisms of ossification, with the ultimate goal to improve membrane design, material, and application techniques, as well as helping to guide physical therapy recommendations for patients receiving the implant, all of which are crucial for clinical translation. Given the promise of using autologous or potentially allogenic periosteal strips or periosteum-derived cells to enhance tissue generation, more studies are needed to elucidate the regenerative capacity of these factors. This study elucidates the behavior of stem cells in the context of their environment, ultimately paving the way to understand and then to control tissue genesis at multiple length and time scales. Understanding mechanisms underlying nature's emergent properties is a first step in applying nature's principles to the engineering of smart, advanced materials, including tissues. Finally, multimodal, high-resolution imaging of anatomical cross-sections at cellular scale resolution enables not only in situ assessment of tissue genesis by stem cells but also assessment of interactions of cells with absorbable and nonabsorbable materials commonly used in reconstructive surgery [57]. Cutting-edge imaging modalities will enable seamless imaging of the periosteum and its cellular inhabitants, from the organ to subcellular length scale, enabling observation of PDCs in their native milieu and in interaction with novel functional materials of the future [77–78].

Conclusion

In sum, the artificial periosteum provides a promising vehicle for directional delivery of factors native to the periosteum for healing of tissue defects. Surgical use of the membrane could speed patient recovery and reduce complications as well as costs associated with current treatments. Future studies aiming to unravel specific extracellular matrix proteins conducive to tissue genesis and healing and expanding the intrinsic regenerative capacity of PDCs will further expand the translational potential of the periosteum and associated periosteum substitutes.

Acknowledgments

The study was supported with grants from the Case Coulter Translational Research Partnership, the Whitaker International Fellows and Scholars Program, the Alexander von Humboldt Foundation, The Christopher Columbus Foundation and U.S. Chamber of Commerce, and the Paul Trainor Foundation. We thank Drs. Sheronica James and R. Matthew Miller and Frau Gita Ziegleder for their assistance with the project. The intellectual property describing the periosteum substitute membrane was patented on March 15, 2015 [47].

Author Contributions

S.R.M.: conception and design, collection and assembly of data, data analysis and interpretation, manuscript writing; C.H. and N.Y.C.Y.: data interpretation, manuscript writing; R.M.W.: collection and assembly of data; U.R.K.: provision of study material, experimental surgery, design of periosteum substitute; S.M.: data analysis and interpretation, final approval of manuscript; M.L.K.T.: conception and design, design of periosteum substitute, data analysis and interpretation, manuscript writing, final approval of manuscript.

Disclosure of Potential Conflicts of Interest

U.R.K. has uncompensated intellectual property rights. M.L.K.T. has uncompensated intellectual property rights (for a U.S. patent granted for Multilayer Surgical Membrane that mimics the periosteum) and is a director of an unrelated start-up company. The other authors indicated no potential conflicts of interest.

REFERENCES

1 Lazzeri D, Gatti GL, Romeo G et al. Bone regeneration and periosteoplasty: a 250-year-long history. Cleft Palate Craniofac J 2009;46: 621–628.

2 Duhamel HL. Sur une racine qui a la faculté de tiendre en rouge les os des animaux vivants. Mem Acad Roy des Sciences 1739;52:1.

3 Syme J. On the power of the periosteum to form new bone. In: Contribution to the Pathology and Practice of Surgery. Edinburgh: Murray & Gibb, 1848.

4 de Cristoforis M. Dell'importanza del periostio nella rigenerazione delle ossa, nella patologia e chirugia loro: studi esperimentali del dott. Ann Uni Med. Milano: De Cristoforis Malachia, 1862.

5 Gupta SR, Anand R, Diwan S et al. Salvaging recurrent scleral buckle exposure with autologous periosteal patch graft. Retin Cases Brief Rep 2014;8:178–182.

6 Nordin KE, Johansson B. Freie Knochentransplantation bei Defekten in Alveolarkamm nach kieferorthopädischer Einstellung der Maxilla bei Lippen-Kiefer-Gaumenspalten. In: Schuchard K, Wassmund M, eds. Fortschritte der Kiefer- und Gesichtschirurgie. Stuttgart: Georg Thieme Verlag, 1955: 168–171.

7 Skoog T. The use of periosteal flaps in the repair of clefts of the primary palate. Cleft Palate J 1965;2:332–339.

8 Hata Y, Ohmori S. On the experiences of periosteoplasty for the closure of the maxillary cleft. Eur J Plast Surg 1979;5:33–43.

9 Massei A. Reconstruction of cleft maxilla with periosteoplasty. Scand J Plast Reconstr Surg 1986;20:41–44.

10 Rintala AE, Ranta R. Periosteal flaps and grafts in primary cleft repair: A follow-up study. Plast Reconstr Surg 1989;83:17–24.

11 Dixit UB, Kelly KM, Squier CA et al. Periosteum in regeneration of palatal defects. Cleft Palate Craniofac J 1995;32:228–234.

12 Rahpeyma A, Khajehahmadi S. The last resort for reconstruction of nasal floor in difficult-to-repair alveolar cleft cases: A retrospective study. J Craniomaxillofac Surg 2014; 42:995–999.

13 Passanezi E, Alves ME, Janson WA et al. Periosteal activation and root demineralization associated with the horizontal sliding flap. J Periodontol 1979;50:384–386.

14 Gamal AY, Mailhot JM. A novel marginal periosteal pedicle graft as an autogenous guided tissue membrane for the treatment of intrabony periodontal defects. J Int Acad Periodontol 2008;10:106–117.

15 Hazzaa HH, El Adawy H, Magdi HM. A novel surgical approach for treatment of class II furcation defects using marginal periosteal membrane. J Int Acad Periodontol 2015;17: 20–31.

16 Choi YR, Hong CG. Repair of tibialis anterior muscle herniation using periosteum. Orthopedics 2014;37:748–750.

17 Nakahara H, Goldberg VM, Caplan AI. Culture-expanded human periosteal-derived cells exhibit osteochondral potential in vivo. J Orthop Res 1991;9:465–476.

18 O'Driscoll SW. Articular cartilage regeneration using periosteum. Clin Orthop Relat Res 1999;367(suppl):S186–S203.

19 Wakitani S, Imoto K, Yamamoto T et al. Human autologous culture expanded bone marrow mesenchymal cell transplantation for repair of cartilage defects in osteoarthritic knees. Osteoarthritis Cartilage 2002;10:199–206.

20 Wakitani S, Mitsuoka T, Nakamura N et al. Autologous bone marrow stromal cell transplantation for repair of cartilage defects in human patellae: Two case reports. Cell Transplant 2004;13:595–600.

21 Brittberg M, Sjögren-Jansson E, Thornemo M et al. Clonal growth of human articular cartilage and the functional role of the periosteum in chondrogenesis. Osteoarthritis Cartilage 2005;13:146–153.

22 Fu WL, Ao YF, Ke XY et al. Repair of large full-thickness cartilage defect by activating endogenous peripheral blood stem cells and autologous periosteum flap transplantation combined with patellofemoral realignment. Knee 2014;21:609–612.

23 McCarthy HS, Roberts S. A histological comparison of the repair tissue formed when using either Chondrogide(®) or periosteum during autologous chondrocyte implantation. Osteoarthritis Cartilage 2013;21:2048–2057.

24 Moradi B, Schönit E, Nierhoff C et al. First-generation autologous chondrocyte implantation in patients with cartilage defects of the knee: 7 to 14 years' clinical and magnetic resonance imaging follow-up evaluation. Arthroscopy 2012;28:1851–1861.

25 Tovi F, Gittot A. Sternocleidomastoid myoperiosteal flap for the repair of laryngeal and tracheal wall defects. Head Neck Surg 1983;5:447–451.

26 Cohen RC, Filler RM, Konuma K et al. The successful reconstruction of thoracic tracheal defects with free periosteal grafts. J Pediatr Surg 1985;20:852–858.

27 Knothe UR, Springfield DS. A novel surgical procedure for bridging of massive bone defects. World J Surg Oncol 2005;3:7.

28 Verdugo F, Simonian K, D'Addona A et al. Human bone repair after mandibular symphysis block harvesting: a clinical and tomographic study. J Periodontol 2010;81:702–709.

29 Bertram FW, Harrison J, Freeman R. The role of the periosteum in healing a large structural defect following sequestrectomy. Trop Doct 2011;41:54–56.

30 Jacobsen FS. Periosteum: Its relation to pediatric fractures. J Pediatr Orthop B 1997;6: 84–90.

31 Bartlett CS 3rd, Weiner LS, Yang EC. Treatment of type II and type III open tibia fractures in children. J Orthop Trauma 1997;11: 357–362.

32 Evans SF, Parent JB, Lasko CE et al. Periosteum, bone's "smart" bounding membrane, exhibits direction-dependent permeability. J Bone Miner Res 2013;28:608–617.

33 Evans SF, Chang H, Knothe Tate ML. Elucidating multiscale periosteal mechanobiology: A key to unlocking the smart properties and regenerative capacity of the periosteum? Tissue Eng Part B Rev 2013;19:147–159.

34 McBride SH, Evans SF, Knothe Tate ML. Anisotropic mechanical properties of ovine femoral periosteum and the effects of cryopreservation. J Biomech 2011;44:1954–1959.

35 Yiannakopoulos CK, Kanellopoulos AD, Trovas GP et al. The biomechanical capacity of the periosteum in intact long bones. Arch Orthop Trauma Surg 2008;128:117–120.

36 Lai X, Price C, Lu XL et al. Imaging and quantifying solute transport across periosteum: Implications for muscle-bone crosstalk. Bone 2014;66:82–89.

37 De Bari C, Dell'Accio F, Luyten FP. Human periosteum-derived cells maintain phenotypic stability and chondrogenic potential throughout expansion regardless of donor age. Arthritis Rheum 2001;44:85–95.

38 Chang H, Docheva D, Knothe UR et al. Arthritic periosteal tissue from joint replacement surgery: A novel, autologous source of stem cells. STEM CELLS TRANSLATIONAL MEDICINE 2014; 3:308–317.

39 Moore SR, Milz S, Knothe Tate ML. Periosteal thickness and cellularity in mid-diaphyseal cross-sections from human femora and tibiae of aged donors. J Anat 2014;224:142–149.

40 McBride SH, Dolejs S, Brianza S et al. Net change in periosteal strain during stance shift loading after surgery correlates to rapid de novo bone generation in critically sized defects. Ann Biomed Eng 2011;39:1570–1581.

41 Yu NYC, O'Brien CA, Slapetova I, Whan RM, Knothe Tate ML. Live tissue imaging to elucidate mechanical modulation of stem cell niche quiescence. STEM CELLS TRANSLATIONAL MEDICINE 2015 (in press).

42 Knothe Tate ML, Ritzman TF, Schneider E et al. Testing of a new one-stage bone-transport surgical procedure exploiting the periosteum for the repair of long-bone defects. J Bone Joint Surg Am 2007;89:307–316.

43 Knothe UR, Dolejs S, Matthew Miller R et al. Effects of mechanical loading patterns, bone graft, and proximity to periosteum on bone defect healing. J Biomech 2010;43: 2728–2737.

44 Knothe Tate ML, Chang H, Moore SR et al. Surgical membranes as directional delivery devices to generate tissue: Testing in an ovine critical sized defect model. PLoS One 2011;6: e28702.

45 Knothe Tate ML, Dolejs S, McBride SH et al. Multiscale mechanobiology of de novo bone generation, remodeling and adaptation of autograft in a common ovine femur model. J Mech Behav Biomed Mater 2011; 4:829–840.

46 McBride SH, Dolejs S, Knothe U et al. Major and minor centroidal axes serve as objective, automatable reference points to test mechanobiological hypotheses using histomorphometry. J Biomech 2011;44:1205–1208.

47 Knothe Tate M, Knothe U. Multilayer surgical membrane, U.S. patent US20130211540 A1, issued March 15, 2015.

48 Knothe Tate ML, Knothe UR. Composition and method for inducing bone growth and healing, U.S. patent US7879107 B2, 2011.

49 Horton WA, Dwyer C, Goering R et al. Immunohistochemistry of types I and II collagen in undecalcified skeletal tissues. J Histochem Cytochem 1983;31:417–425.

50 Chang H, Knothe Tate ML. Concise review: The periosteum: Tapping into a reservoir

of clinically useful progenitor cells. STEM CELLS TRANSLATIONAL MEDICINE 2012;1:480–491.

51 Merritt FJW, Erinc AM, Knothe Tate ML. Periosteum regenerates on periosteum-denuded, transported bone segment. Trans Orthop Res 2012;37:1570.

52 Bourke H, Sandison A, Hughes S et al. Vascular endothelial growth factor (VEGF) in human periosteum–normal expression and response to fracture. J Bone Joint Surg Br 2003;85:4.

53 Chanavaz M. Anatomy and histophysiology of the periosteum: Quantification of the periosteal blood supply to the adjacent bone with 85Sr and gamma spectrometry. J Oral Implantol 1995;21:214–219.

54 Colnot C. Skeletal cell fate decisions within periosteum and bone marrow during bone regeneration. J Bone Miner Res 2009;24:274–282.

55 Yu YY, Lieu S, Lu C et al. Bone morphogenetic protein 2 stimulates endochondral ossification by regulating periosteal cell fate during bone repair. Bone 2010;47:65–73.

56 Evans SF, Docheva D, Bernecker A et al. Solid-supported lipid bilayers to drive stem cell fate and tissue architecture using periosteum derived progenitor cells. Biomaterials 2013; 34:1878–1887.

57 Knothe Tate ML, Detamore M, Capadona JR et al. Engineering and commercialization of human-device interfaces, from bone to brain. Biomaterials 2016;95:35–46.

58 Naujoks C, Von Beck FP, Langenbach F et al. Biocompatibility of membranes with unrestricted somatic stem cells. In Vivo 2013;27: 41–47.

59 Takata T, Wang HL, Miyauchi M. Migration of osteoblastic cells on various guided bone regeneration membranes. Clin Oral Implants Res 2001;12:332–338.

60 Duarte Campos DF, Blaeser A, Buellesbach K et al. Bioprinting organotypic hydrogels with improved mesenchymal stem cell remodeling and mineralization properties for bone tissue engineering. Adv Healthc Mater 2016;5: 1336–1345.

61 Kuzyk PR, Li R, Zdero R et al. The effect of intramedullary reaming on a diaphyseal bone defect of the tibia. J Trauma 2011;70: 1248–1256.

62 Schmid J, Hämmerle CH, Olah AJ et al. Membrane permeability is unnecessary for guided generation of new bone. An experimental study in the rabbit. Clin Oral Implants Res 1994;5:125–130.

63 Moore SR, Saidel GM, Knothe U et al. Mechanistic, mathematical model to predict the dynamics of tissue genesis in bone defects via mechanical feedback and mediation of biochemical factors. PLOS Comput Biol 2014;10: e1003604.

64 Foolen J, van Donkelaar C, Nowlan N et al. Collagen orientation in periosteum and perichondrium is aligned with preferential directions of tissue growth. J Orthop Res 2008;26: 1263–1268.

65 Douglas T, Heinemann S, Bierbaum S et al. Fibrillogenesis of collagen types I, II, and III with small leucine-rich proteoglycans decorin and biglycan. Biomacromolecules 2006; 7:2388–2393.

66 Khouri RK, Koudsi B, Reddi H. Tissue transformation into bone in vivo. A potential practical application. JAMA 1991;266:1953–1955.

67 Endo T. Molecular mechanisms of skeletal muscle development, regeneration, and osteogenic conversion. Bone 2015;80:2–13.

68 Taguchi Y, Amizuka N, Nakadate M et al. A histological evaluation for guided bone regeneration induced by a collagenous membrane. Biomaterials 2005;26:6158–6166.

69 Gugala Z, Gogolewski S. Healing of critical-size segmental bone defects in the sheep tibiae using bioresorbable polylactide membranes. Injury 2002;33(suppl 2):B71–B76.

70 Klaue K, Knothe U, Anton C et al. Bone regeneration in long-bone defects: Tissue compartmentalisation? In vivo study on bone defects in sheep. Injury 2009;40(suppl 4): S95–S102.

71 Buser D, Dula K, Belser U et al. Localized ridge augmentation using guided bone regeneration. 1. Surgical procedure in the maxilla. Int J Periodontics Restorative Dent 1993;13: 29–45.

72 Epari DR, Taylor WR, Heller MO et al. Mechanical conditions in the initial phase of bone healing. Clin Biomech (Bristol, Avon) 2006;21: 646–655.

73 Wallace AL, Draper ER, Strachan RK et al. The vascular response to fracture micromovement. Clin Orthop Relat Res 1994;(301): 281–290.

74 Knothe Tate ML, Falls TD, McBride SH et al. Mechanical modulation of osteochondroprogenitor cell fate. Int J Biochem Cell Biol 2008;40: 2720–2738.

75 Song MJ, Brady-Kalnay SM, McBride SH et al. Mapping the mechanome of live stem cells using a novel method to measure local strain fields in situ at the fluid-cell interface. PLoS One 2012;7:e43601.

76 Song MJ, Dean D, Knothe Tate ML. Mechanical modulation of nascent stem cell lineage commitment in tissue engineering scaffolds. Biomaterials 2013;34:5766–5775.

77 Knothe Tate ML, Zeidler D, Pereira AF et al. Organ-to-cell-scale health assessment using geographical information system approaches with multibeam scanning electron microscopy. Adv Healthc Mater 2016;5:1581–1587.

78 Takata T, Wang HL, Miyauchi M. Migration of osteoblastic cells on various guided bone regeneration membranes. Clin Oral Implants Res 2001;12:332–338.

79 Knothe Tate ML, Fath T. The only constant is change: next generation materials and medical device design for physical and mental health. Adv Healthc Mat 2016 [Epub ahead of print].

See www.StemCellsTM.com for supporting information available online.

